The influence of physical properties of materials used for slide rings on the process of heat transfer in the non-contacting face seals

Slawomir Blasiak [1,*]

[1] Kielce University of Technology, Faculty of Mechatronics and Mechanical Engineering, Department of Mechanical Technology and Metrology, Aleja Tysiaclecia Panstwa Polskiego 7, 25-314 Kielce, Poland

Abstract. The paper presents the results of analytical solution of the model of heat transfer for non-contacting face seals. Comparative analyses were performed for various physical properties of materials used for slide rings. A mathematical model includes a series of differential equations of partial derivatives with generally used boundary conditions, i.e. the Reynold's equation, energy equation and heat transfer equations, which describe the heat transfer in sealing rings with surrounding medium. Heat transfer equation is written in the Cartesian coordinate system and solved using the Green's functions method. Theoretical studies made it possible to draw a number of practical conclusions on the phenomena of heat transfer in the node seal. The presented model will allow more accurate identification of the heat transfer mechanism in the node seal. The results will help to select appropriate materials for sealing rings, depending on operating conditions of non-contacting face seals.

1 Introduction

Sealing technique used in flow machines is one of the key and steadily developing branches of applied research. A wide spectrum of the inter-connected physical phenomena occurring in sealing nodes poses serious problems. Over the past years, many research works considered the results of the bench testing and of the numerical studies obtained via solutions based on complex mathematical models. The scope of the conducted research included, among others, the sealing rings vibration model [1–6], thermal and fluid flow dynamics [7–26], material properties [27–30], measurements and control systems [31–43], as well as the heat transfer in the sealing nodes, the works of: [44–46] but also in experimental studies covering measurements of geometrical quantities and surface structures, materials used [47–52] or studies aimed at measuring temperatures on test rigs [53–55].

The studies published in the above mentioned works are especially important due to the wide range of temperatures for contactless face seals. Manufacturers of the contactless face seals declare working temperature ranges of those components to be between -20 and 220 °C for gas dynamics seals, and between -54 and 650 °C for contactless face seals co-functioning with other media [20] and under extremely different operating parameters [14]. Such a wide range of working temperatures creates a series of problems that researchers have to deal with. Because the assumed height of the radial gap varies by several micrometres, there might occur a rapid evaporation of the working medium in the fluid film. This determines how research is undertaken and conducted. It also determines how to develop improved mathematical models describing the phenomenon of two-phase radial gap flow [29], and how to conduct research on those phenomena under laboratory conditions [41]. By carrying out more specific literature analysis in terms of heat transfer of the contactless face seals, for both the fluid film and co-functioning rings, it is appropriate to mention the works that present complex thermodynamic (THD) and thermo-elastohydrodynamic (TEHD) models, such as the works of: [8] and [13] as well as the works characterized by numerical solutions of the proposed models of heat transfer and thermoelastic deformations of the ring seals [12].

The development of new technologies allows for preparation of materials with physical properties that enable dissipation of huge amounts of heat flux into the environment. It is especially important in cases, where contactless face seals are used in devices that pump hazardous media, such as chemically aggressive or explosive substances whose leakage could lead to contamination of the natural environment or other accidents.

2 Formulation of the problem

Depending on the type of its design, contactless face seal must consist of at least one pair of main rings, i.e.: one stationary (1) and one vibrating (2) ring, with radial gap filled with working medium, the so-called fluid film. The

* Corresponding author: sblasiak@tu.kielce.pl

diagram of the FMR-type (Flexible Mounted Stator) contactless seal is shown in Fig. 1.

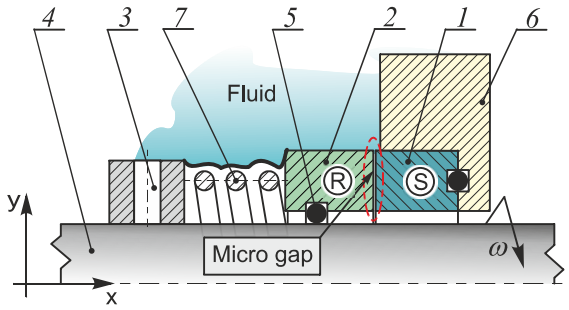

Fig. 1. Diagram of the FMR-type contactless face seal. 1 – Stator, 2 – Rotor, 3 – Connecting element, 4 – Shaft, 5 – O-ring, 6 – Casing, 7 – Spring.

The primary condition that determines proper functioning of the contactless face seals is the maintenance of gap that keeps the co-functioning rings apart by few micrometres. That condition can be met only when balance of forces acting on the rings system is maintained. At this point one should distinguish two main types of forces acting on the susceptibly positioned rotor, i.e. the closing force, which comes mainly from the compression spring, and the opening force generated in the fluid film. The opening force is dependent on the shape of the gap and on the pressure in the fluid film that results from it. The mathematical model of the contactless face seals is commonly known and has been presented in the previous works of the author. At this point, the only cited elements are the primary formulas that govern the processes taking place in the fluid film and ring seals.

Reynolds' single-dimensional (in the radial direction) equation describes pressure layout in the fluid film:

$$\frac{d}{dy}\left(\frac{\rho h(y)^3}{\mu}\frac{dp}{dy}\right)=0 \tag{1}$$

Height of the radial gap for the smooth gliding surface – without modifications:

$$h=h(y)=h_o \tag{2}$$

Temperature layout in the fluid film is determined based on a simplified energy equation:

$$\mu\left(\frac{\partial v_\varphi}{\partial x}\right)^2+\lambda^f\frac{\partial^2 T^f}{\partial x^2}=0 \tag{3}$$

A linear change in the fluid flow v_φ along the height of the fluid film (Couette's Flow) was adopted. Change in the fluid speed by the coordinate x is noted as:

$$\frac{\partial v_\varphi}{\partial x}=\frac{\omega(r_i+y)}{h} \tag{4}$$

Boundary conditions used in the solution of mathematical model are illustrated in Fig. 2:

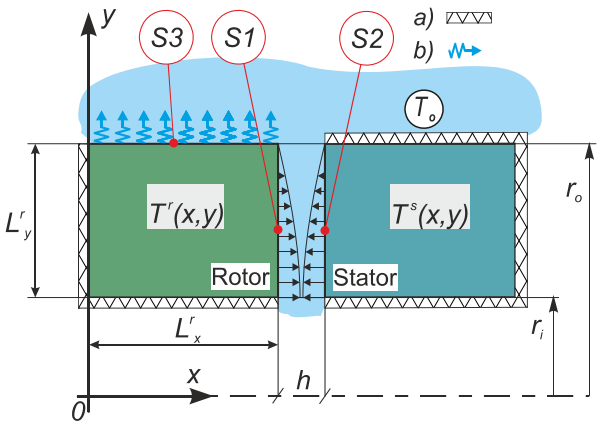

Fig. 2. Heat transfer conditions in the contactless face seal, a) Isolated surfaces, b) Heat transfer through natural convection.

The equality of temperatures– T^r (y) = T^f (y) as well as heat flux: $\lambda^r\left(\frac{\partial T^r}{\partial x}\right)=\lambda^f\left(\frac{\partial T^f}{\partial x}\right)\Big|_{x=0}$ between the main ring and the fluid film was adopted for the *S1* surface. On the *S2* surface – it is assumed similarly that the temperatures of the fluid film and the stationary ring are equal – T^f (y) = T^s (y) for $x = h$, and that the temperature on contact between the fluid film and the stator reaches the maximum value: $\left(\frac{\partial T^f}{\partial x}\right)_{x=h}=0$. A heat transfer through natural convection on the S3 surface was assumed according to the following dependency: $-\lambda^r\frac{\partial T^r}{\partial y}\Big|_{y=L^r_y}=\alpha^r\left(T^r-T_o\right)\Big|_{y=L^r_y}$.

The mathematical model formulated in this way has been solved analytically using the Green's Function Method.

3 Analytical Solution

The first stage of the analytical solution consisted in determining the temperature layouts in the ring seal by outlining the general functions satisfying the Laplace's Equation (5) for both main rings. The solution included the above boundary conditions and employed a coordinate system to simplify analytical calculations.

$$\frac{\partial^2\theta}{\partial x^2}+\frac{\partial^2\theta}{\partial y^2}=0 \tag{5}$$

Further part of the study will include analytical solution for the stator. Calculations for the rotor are characterized with full analogy, and hence final formulas will be quoted. The separation of variables method was used in the course of solving the Laplace's Equation. Two harmonic functions *X(x)* and *Y(y)* were introduced, being added that each of these had only one variable, while the sought temperature layout $\theta(x,y)$ was presented as their product:

$$\theta(x,y)=X(x)\cdot Y(y) \tag{6}$$

After placing the adopted functions in the differential equation (5), the outcome was: $\frac{X''(x)}{X(x)} = \beta^2$ and $\frac{Y''(y)}{Y(y)} = \gamma^2$. After the transformation, two independent equations were determined:

$$X''(x) + \beta^2 X(x) = 0 \tag{7}$$
$$Y''(y) + \gamma^2 Y(y) = 0 \tag{8}$$

General solutions of the (7) and (8) equations take the overall shape of:

$$X(x) = A_m \cos(\beta_m x) + B_m \sin(\beta_m x) \tag{9}$$
$$Y(y) = C_n \cos(\gamma_n y) + D_n \sin(\gamma_n y) \tag{10}$$

By implementing the $\theta|_{x=0} = 0$ for $0 < y < L_y$ condition in the equation (9), it has been determined that the coefficient A_m amounts to 0. Subsequently, by taking into account the general condition: $\left.\frac{\partial\theta}{\partial x}\right|_{x=L_x} = 0$ for $0 < y < L_y$ it can be assumed that the solutions for the equation $\beta_m B_m \cos(\beta_m L_x) = 0$ are the following values: $\beta_m = \frac{\left(m - \frac{1}{2}\right)\pi}{L_x}$ for m=1,2,3,…. Therefore, the equation (9) takes the following form:

$$X(x) = \sum_{m=1}^{\infty} B_m \sin(\beta_m x) \tag{11}$$

By implementing the boundary condition: $\left.\frac{\partial\theta}{\partial y}\right|_{y=0} = 0$ for $0 < x < L_x$ in the dependency (10), the outcome was that D_n = 0. By further inserting the boundary condition: $\left.\frac{\partial\theta}{\partial y}\right|_{y=L_y} = 0$ for $0 < x < L_x$ into the equation (10), the coefficient γ_n took the value of $\gamma_n = \frac{n\pi}{L_y}$ for n=1,2,3,…. Whereas the equation (10) adopted the form of:

$$Y(y) = \sum_{m=1}^{\infty} C_n \cos(\gamma_n y) \tag{12}$$

By using the equations (11) and (12), the dependency (6) describing the temperature layout in the stator has been determined as: $c_{n,m} = B_m C_n$:

$$\theta(x,y) = \sum_{m=1}^{\infty}\sum_{n=1}^{\infty} c_{n,m} \sin(\beta_m x)\cos(\gamma_n y) \tag{13}$$

The $c_{n,m}$ coefficient has been determined similarly, as in the work of [56].

$$c_{n,m} = \frac{\int_0^{L_x}\int_0^{L_y} \theta(x',y')\sin(\beta_m x')\cos(\gamma_n y')\,dy'\,dx'}{\int_0^{L_x}\sin^2(\beta_m x)\,dx \int_0^{L_y}\cos^2(\gamma_n y)\,dy} \tag{14}$$

The temperature layout in the cross-section of the stator has been noted as:

$$\theta^s(x,y) = \int_0^{L_x}\int_0^{L_y} \frac{\partial G^s(x,y \mid x',y')}{\partial x'}\theta(x',y')\,dy'\,dx' \tag{15}$$

The Green's Function for the $G^s(x, y \mid x', y')$ is presented by the following dependency:

$$G^s(x,y \mid x',y') = \frac{4}{L_x L_y} \sum_{m=1}^{\infty}\sum_{n=1}^{\infty} \frac{\sin(\beta_m^s x)\sin(\beta_m^s x')\cos(\gamma_n^s y)\cos(\gamma_n^s y')}{\left(\beta_m^{s\,2} + \gamma_n^{s\,2}\right)} + \frac{2}{L_x L_y}\sum_{m=1}^{\infty} \frac{\sin(\beta_m^s x)\sin(\beta_m^s x')}{\beta_m^{s\,2}} \tag{16}$$

In the following part of the work, the derivative of the Green's Function in relation to the x' coordinate has been determined:

$$\left.\frac{\partial G^s(x,y \mid x',y')}{\partial x'}\right|_{x'=0} = \frac{\partial}{\partial x'}\left(\frac{4}{L_x L_y}\sum_{m=1}^{\infty}\sum_{n=1}^{\infty} \frac{\sin(\beta_m^s x)\sin(\beta_m^s x')\cos(\gamma_n^s y)\cos(\gamma_n^s y')}{\left(\beta_m^{s\,2} + \gamma_n^{s\,2}\right)} + \frac{2}{L_x L_y}\sum_{m=1}^{\infty} \frac{\sin(\beta_m^s x)\sin(\beta_m^s x')}{\beta_m^{s\,2}}\right)$$

In the x' = 0 point, it takes the value of:

$$\left.\frac{\partial G}{\partial x'}\right|_{x'=0} = \left(\begin{array}{l} \cos\left(\frac{n\pi}{L_y}y\right)\cos\left(\frac{n\pi}{L_y}y'\right)\cdot \\ \cdot\frac{4}{L_y\pi}\sum_{n=1}^{\infty} \frac{\left(m-\frac{1}{2}\right)\sin\left(\frac{\left(m-\frac{1}{2}\right)\pi}{L_x}x\right)}{\sum_{m=1}^{\infty}\left(\left(m-\frac{1}{2}\right)^2 + \left(\frac{L_x n}{L_y}\right)^2\right)} + \\ + \frac{2}{L_y\pi}\sum_{m=1}^{\infty} \frac{\left(m-\frac{1}{2}\right)\sin\left(\frac{\left(m-\frac{1}{2}\right)\pi}{L_x}x\right)}{\left(m-\frac{1}{2}\right)^2} \end{array}\right) \tag{18}$$

Using the substitution:

$$\sum_{m=1}^{\infty}\frac{\left(m-\frac{1}{2}\right)\sin\left(\frac{\left(m-\frac{1}{2}\right)\pi}{L_x}x\right)}{\left(\left(m-\frac{1}{2}\right)^2+\left(\frac{L_x n}{L_y}\right)^2\right)}=\frac{\pi}{2}\frac{\sinh\left(\frac{L_x n\pi}{L_y}\left(1-\frac{x}{L_x}\right)\right)}{\sinh\left(\frac{L_x n\pi}{L_y}\right)} \quad (19)$$

In the end, the dependency describing the temperature layout in the stator takes the following form:

$$\theta^s(x,y)=\frac{2}{L_y}\sum_{n=1}^{\infty}\cos\left(\frac{n\pi}{L_y}y\right)\frac{\sinh\left(\frac{L_x n\pi}{L_y}\left(1-\frac{x}{L_x}\right)\right)}{\sinh\left(\frac{L_x n\pi}{L_r}\right)}\cdot$$
$$\cdot\int_0^{L_y}\left(\theta(\mathrm{x',y'})\big|_{x'=0}\cos\left(\frac{n\pi}{L_y}y'\right)\right)dy'+ \quad (20)$$
$$+\frac{2}{L_y\pi}\sum_{m=1}^{\infty}\frac{\sin\left(\frac{\left(m-\frac{1}{2}\right)\pi}{L_x}x\right)}{\left(m-\frac{1}{2}\right)}\int_0^{L_y}\left(\theta(\mathrm{x',y'})\big|_{x'=0}\right)dy'$$

By using the dependencies set out in the work of [56], the Green's Function for the rotor takes the following form:

$$G^r(x,y\,|\,x',y')=\frac{2}{L_x}\sum_{m=1}^{\infty}\sum_{n=1}^{\infty}\frac{2\left(\gamma_n^{r2}+\left(\frac{\alpha^r}{\lambda^r}\right)^2\right)}{L_y\left(\gamma_n^{r2}+\left(\frac{\alpha^r}{\lambda^r}\right)^2\right)+\left(\frac{\alpha^r}{\lambda^r}\right)}\cdot$$
$$\cdot\frac{\cos\left(\beta_m^r x\right)\cos\left(\beta_m^r x'\right)\cos\left(\gamma_n^r y\right)\cos\left(\gamma_n^r y'\right)}{\left(\gamma_n^{r2}+\beta_m^{r2}\right)} \quad (21)$$
$$+\frac{1}{L_x}\sum_{n=1}^{\infty}\frac{2\left(\gamma_n^{r2}+\left(\frac{\alpha^r}{\lambda^r}\right)^2\right)}{L_y\left(\gamma_n^{r2}+\left(\frac{\alpha^r}{\lambda^r}\right)^2\right)+\left(\frac{\alpha^r}{\lambda^r}\right)}\frac{\cos\left(\gamma_n^r y\right)\cos\left(\gamma_n^r y'\right)}{\left(\gamma_n^{r2}\right)}$$

The values of the coefficient β_m^r are $\beta_m^r=\frac{m\cdot\pi}{L_x}$ for m=1,2,3… The values of the coefficient γ_n^r were determined by solving the equation $\gamma_n^r\tan\left(\gamma_n^r L_y\right)=\frac{\alpha^r}{\lambda^r}$. This is a transcendental equation, and it can be solved by iteration, where λ^r is the coefficient of rotor heat conductivity. The temperature layout in the rotor has been formulated in way convenient for use in mathematical calculations:

$$\theta^r(x,y)=\frac{2}{L_x}\sum_{m=1}^{\infty}\sum_{n=1}^{\infty}\frac{2\left(\gamma_n^{r2}+\left(\frac{\alpha^r}{\lambda^r}\right)^2\right)}{L_y\left(\gamma_n^{r2}+\left(\frac{\alpha^r}{\lambda^r}\right)^2\right)+\left(\frac{\alpha^r}{\lambda^r}\right)}\cdot$$
$$\cdot\frac{\cos\left(\beta_m^r x\right)\cos\left(\beta_m^r L_x\right)\cos\left(\gamma_n^r y\right)}{\left(\gamma_n^{r2}+\beta_m^{r2}\right)}\cdot\int_0^{L_x}\left(\frac{d\theta(\mathrm{x',y'})}{dx}\bigg|_{x'=Lx}\cos\left(\gamma_n^r y'\right)\right)dy'+$$
$$+\frac{1}{L_x}\sum_{n=1}^{\infty}\frac{2\left(\gamma_n^{r2}+\left(\frac{\alpha^r}{\lambda^r}\right)^2\right)}{L_y\left(\gamma_n^{r2}+\left(\frac{\alpha^r}{\lambda^r}\right)^2\right)+\left(\frac{\alpha^r}{\lambda^r}\right)}\frac{\cos\left(\gamma_n^r y\right)}{\left(\gamma_n^{r2}\right)}\cdot$$
$$\int_0^{L_y}\left(\frac{d\theta(\mathrm{x',y'})}{dx}\bigg|_{x'=Lx}\cos\left(\gamma_n^r y'\right)\right)dy' \quad (22)$$

The further part of the study involved an analysis regarding how physical properties of materials used for manufacturing of the ring seals influence the heat transfer in the fluid film-main rings system.

4 Results and Discussion

Numerical calculations of the heat transfer in mechanical seals have been conducted with the assumption that the stator is made of resin-impregnated carbon, whereas the rotor, whose properties are compiled in Table 1, is made of the most commonly used materials in manufacturing ring seals.

Table 1. Properties of the materials used for ring seals manufacturing.

Material	Thermal expansion coefficient α [10^{-6} K^{-1}] for 20 °C	Thermal conductivity [W m^{-1} K^{-1}]	Thermal shock resistance [°C]
Resin-impregnated carbon	5.0	14	200
Chemically bound silicon carbide (SiC-Si)	4.4	120	250
Sintered silicon carbide SiC	4.1	100	250
Tungsten carbide (WC)	4.8	70	300
Ceramics (AL203)	7.4-7.6	40	150
Metallized carbon graphite (SCG-M)	3.7	25	250

The parameters from Table 2 were adopted for the purpose of calculations.

Table 2. Geometry- and performance-related parameters.

Geometry and performance-related parameters	
Inner radius r_i	0.040 *(m)*
Outer radius r_o	0.045 *(m)*
Thickness of the rings	0.005 *(m)*
Angular velocity ω	650 (*rad/s*)
Fluid temperature T_o	20 (^oC)
Fluid thermal conductivity λf	0.65 ($W\ m^{-1}\ K^{-1}$)
Convection coefficient (water) α	18 000 ($W\ m^{-2}\ K^{-1}$)
Nominal clearance height h_o	$1{\cdot}10^{-6}$ *(m)*

In Table 2, the working medium is water with temperature of 20 °C on the process side – T_o. It has been assumed that the external radius and the internal radius have the length of 45 mm and 40 mm respectively, for both co-functioning ring seals. A radial gap with the height of 1 μm was used in the calculations.

Fig. 3 presents the temperature layouts in the cross-sections of ring seals and fluid film on the example of silicon carbide (SiC-Si) and metallized carbon graphite, in other words, materials with the highest and the lowest coefficient of heat conductivity λ (according to the parameters of Table 1).

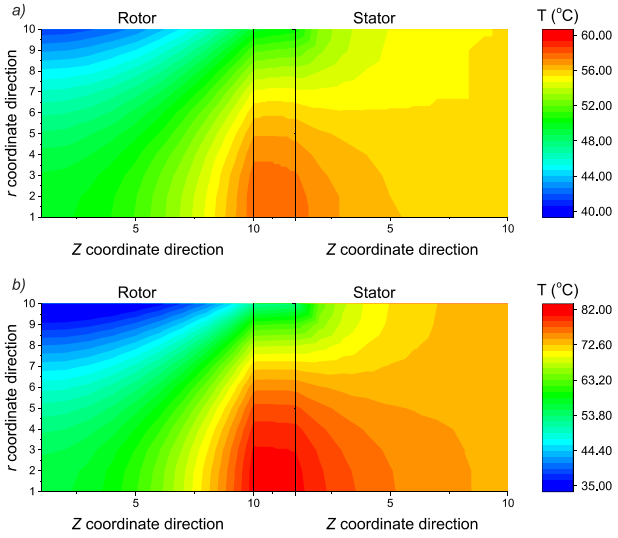

Fig. 3. Temperature distribution in the fluid film and sealing rings for, a) Chemically bound silicon carbide (SiC-Si), b) Metallized carbon graphite.

It can be observed (Fig. 3a) that the rotor, made of a material with high heat conductivity λ, has the maximum temperature lower by 22 °C in the fluid film-ring seals system.

The next figure presents the temperature changes in the radial direction on the verge of the rotating ring and the fluid film.

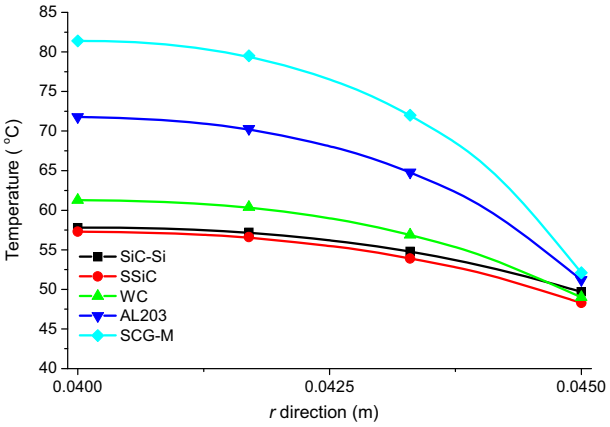

Fig. 4. Temperature distribution in the fluid film-rotor interface

The analysis of the results shown in Fig. 4 was followed by a determination of the smallest differences in temperature layouts of materials with similar physical properties. This concerns chemically bound silicon carbide and sintered silicon carbide. The thermal resistance of the whole studied system increases when the heat transfer coefficient decreases.

5 Conclusion

The main task of the contactless face seals is to keep tightness, regardless of external conditions. There is a close relation between the geometry of the radial gap and the occurrence of a leakage. The major factors connecting the above mentioned parameters are any deformations caused by uneven temperature layout in the ring seals. A development of more precise mathematical models and calculation apparatuses, in the course of the layout design process, will allow to develop the temperature of the rings-fluid film system. That will allow researchers and constructors to estimate the temperature range and select proper materials for the manufacture of ring seals. This knowledge, in turn, will lead to the achievement of high reliability and a long operational life of the developed structures.

Nomenclature

$h(y)$ – clearance geometry in the y direction,
h_o – nominal clearance height,
T^i –temperature,
T_o – temperature of the surrounding fluid,
$i = f,r,s$ – fluid, rotor and stator respectively.

Greeks

α – convection coefficient,
λ^r – thermal conductivity for the rotor,
μ – dynamic viscosity,
ω – angular velocity,
ρ – density.

References

1. D. Gapinski, I. Krzysztofik, (IEEE, 345 E 47TH ST, NEW YORK, NY 10017 USA, 2014).
2. D. Gapinski, I. Krzysztofik, Z. Koruba, *J. Theor. Appl. Mech.* **52** (3) (2014), 629–639.
3. D. Janecki, L. Cedro, J. Zwierzchowski, *Metrol. Meas. Syst.* **22** (2) (2015), 289–302.
4. Z. Koruba, I. Krzysztofik, *Proc. Inst. Mech. Eng. PART K-JOURNAL MULTI-BODY Dyn.* **227** (K1) (2013), 12–16.
5. I. Krzysztofik, (ACAD SCI CZECH REPUBLIC, INST THERMOMECHANICS, DOLEJSKOVA 5, PRAGUE 8, 182 00, CZECH REPUBLIC, 2016).
6. I. Krzysztofik, Z. Koruba, *J. Appl. Math.* (2014),.
7. S. Blasiak, J.E. Takosoglu, P.A. Laski, (ACAD SCI CZECH REPUBLIC, INST THERMOMECHANICS, DOLEJSKOVA 5, PRAGUE 8, 182 00, CZECH REPUBLIC, Svratka, CZECH REPUBLIC, 2014).
8. S. Blasiak, *J. Therm. Sci. Technol.* **10** (1) (2015), JTST0016-JTST0016.
9. S. Blasiak, C. Kundera, *Procedia Eng.* **39** (2012), 315–326.
10. S. Blasiak, C. Kundera, J. Bochnia, *Procedia Eng.* **39** (2012), 366–378.
11. S. Blasiak, A. Pawinska, *Int. J. Heat Mass Transf.* **90** (2015), 710–718.
12. S. Blasiak, J.E. Takosoglu, P.A. Laski, *J. Therm. Sci. Technol.* **9** (2) (2014), JTST0011-JTST0011.
13. N. Brunetiere, *Proc. Inst. Mech. Eng. PART J-JOURNAL Eng. Tribol.* **224** (J12) (2010), 1221–1233.
14. S. Kavinprasad, S. Shankar, M. Karthic, *Ind. Lubr. Tribol.* **67** (2) (2015), 124–132.
15. P.A. Laski, (ACAD SCI CZECH REPUBLIC, INST THERMOMECHANICS, DOLEJSKOVA 5, PRAGUE 8, 182 00, CZECH REPUBLIC, 2016).
16. P.A. Laski, J.E. Takosoglu, S. Blasiak, (ACAD SCI CZECH REPUBLIC, INST THERMOMECHANICS, DOLEJSKOVA 5, PRAGUE 8, 182 00, CZECH REPUBLIC, 2014).
17. P.A. Laski, J.E. Takosoglu, S. Blasiak, *Rob. Auton. Syst.* **72** (2015), 59–70.
18. S.C. Lee, X.L. Zheng, *Comput. Fluids*. **88** (2013), 326–333.
19. Y. Liu, W. Liu, Y. Li, X. Liu, Y. Wang, *Tribol. Int.* **90** (2015), 43–54.
20. X. Meng, S. Bai, X. Peng, *J. ZHEJIANG Univ. A*. **15** (3) (2014), 172–184.
21. A.P. Nyemeck, N. Brunetiere, B. Tournerie, *Tribol. Trans.* **58** (5) (2015), 836–848.
22. M.D. Pascovici, I. Etsion, *ASME J. Tribol.* **1992** (vol.114) (1992), 639–645.
23. D.S. Pietrala, (ACAD SCI CZECH REPUBLIC, INST THERMOMECHANICS, DOLEJSKOVA 5, PRAGUE 8, 182 00, CZECH REPUBLIC, 2016).
24. T. Wang, W. Huang, X. Liu, Y. Li, Y. Wang, *Tribol. Int.* **72** (2014), 90–97.
25. G. Zhang, W. Zhao, *Tribol. Lett.* **53** (2) (2014), 497–509.
26. H. Zhang, R.G. Landers, B.A. Miller, *J. Dyn. Syst. Meas. Control. ASME*. **132** (4) (2010),.
27. M. Blasiak, (ACAD SCI CZECH REPUBLIC, INST THERMOMECHANICS, DOLEJSKOVA 5, PRAGUE 8, 182 00, CZECH REPUBLIC, 2016).
28. J. Bochnia, *Procedia Eng.* **39** (0) (2012), 98–110.
29. J. Bochnia, T. Kozior, *Solid State Phenom.* **223** (2014), 199–208.
30. M. Blasiak, R. Kotowski, *Prz. Elektrotechniczny*. **85** (12) (2009), 40–43.
31. S. Adamczak, J. Bochnia, B. Kaczmarska, *Metrol. Meas. Syst.* **22** (1) (2015), 127–138.
32. S. Adamczak, J. Bochnia, B. Kaczmarska, *Metrol. Meas. Syst.* **21** (3) (2014), 553–560.
33. G.F. Bracha, (ACAD SCI CZECH REPUBLIC, INST THERMOMECHANICS, DOLEJSKOVA 5, PRAGUE 8, 182 00, CZECH REPUBLIC, 2016).
34. D. Janecki, J. Zwierzchowski, L. Cedro, *Bull. POLISH Acad. Sci. Sci.* **63** (3) (2015), 771–779.
35. J.E. Takosoglu, R.F. Dindorf, P.A. Laski, *Int. J. Adv. Manuf. Technol.* **40** (3–4) (2009), 349–361.
36. J.E. Takosoglu, P.A. Laski, S. Blasiak, *Proc. Inst. Mech. Eng. Part I J. Syst. Control Eng.* **226** (10) (2012), 1335–1343.
37. J.E. Takosoglu, P.A. Laski, S. Blasiak, (ACAD SCI CZECH REPUBLIC, INST THERMOMECHANICS, DOLEJSKOVA 5, PRAGUE 8, 182 00, CZECH REPUBLIC, 2014).
38. J.E. Takosoglu, P.A. Laski, S. Blasiak, G. Bracha, D. Pietrala, *Meas. Control*. **49** (2) (2016), 62–71.
39. R. Trochimczuk, T. Kuźmierowski, *Int. J. Appl. Mech. Eng.* **19** (2014), 841.
40. R. Trochimczuk, *Int. J. Appl. Mech. Eng.* **19** (2014), 771.
41. R. Trochimczuk, in: Mechatron. Syst. Mater. IV, 2013: pp. 3–8.
42. R. Trochimczuk, M. Gawrysiak, in: Gosiewski, Z and Kulesza, Z (Ed.), Mechatron. Syst. Mater. III, 2009: pp. 107–112.
43. J.E. Takosoglu, (ACAD SCI CZECH REPUBLIC, INST THERMOMECHANICS, DOLEJSKOVA 5, PRAGUE 8, 182 00, CZECH REPUBLIC, 2016).
44. Huang Weifeng, Liao Chuanjun, Liu Xiangfeng, Suo Shuangfu, Liu Ying, Wang Yuming, *CHINESE J. Mech. Eng.* **27** (5) (2014), 949–957.
45. S. Bai, C. Ma, X. Peng, S. Wen, *J. Tribol. ASME*. **137** (2) (2015),.
46. C. Ma, S. Bai, X. Peng, *Tribol. Int.* **95** (2016), 44–54.
47. E. Miko, L. Nowakowski, *Procedia Eng.* **39** (2012), 405–413.
48. E. Miko, L. Nowakowski, *Procedia Eng.* **39** (2012), 395–404.
49. L. Nowakowski, M. Miesikowska, M. Blasiak, (ACAD SCI CZECH REPUBLIC, INST THERMOMECHANICS, DOLEJSKOVA 5, PRAGUE 8, 182 00, CZECH REPUBLIC, 2016).
50. L. Nowakowski, E. Miko, M. Skrzyniarz, (ACAD SCI CZECH REPUBLIC, INST THERMOMECHANICS, DOLEJSKOVA 5, PRAGUE 8, 182 00, CZECH REPUBLIC, 2016).
51. L. Nowakowski, M. Wijas, (ACAD SCI CZECH REPUBLIC, INST THERMOMECHANICS, DOLEJSKOVA 5, PRAGUE 8, 182 00, CZECH REPUBLIC, 2016).
52. J. Zwierzchowski, (ACAD SCI CZECH REPUBLIC, INST THERMOMECHANICS, DOLEJSKOVA 5, PRAGUE 8, 182 00, CZECH REPUBLIC, 2016).
53. M. Piasecka, *Int. J. Heat Mass Transf.* **81** (2015), 114–121.
54. M. Piasecka, *Int. J. Refrig.* **56** (2015), 198–212.
55. M. Piasecka, B. Maciejewska, *Exp. Therm. Fluid Sci.* **68** (2015), 459–467.
56. M.N. Özişik, (2nd ed., Wiley, New York, 1993).